

Single-Virion SARS-CoV-2 Mass Spectrometry in Air by On-Chip Focusing NEMS

R. Tufan Erdoğan^{1,}, Mohammed Alkhaled^{1,*}, Batuhan E. Kaynak^{1,*}, Hadi S. Pisheh^{1,*}, Mehmet Kelleci^{1,*}, Hashim Alhmoud^{1,*}, Ilbey Karakurt^{1,*}, Cenk Yanık², Z. Betül Sen¹, Burak Sari³, Ahmet M. Yağcı⁴, Aykut Özkul^{5,6}, Mehmet Selim Hanay^{1,7,‡}*

¹*Department of Mechanical Engineering, Bilkent University, 06800 Ankara Turkey*

²*Sabancı University, SUNUM Nanotechnology Research and Application Center, 34956 Istanbul Turkey*

³*Faculty of Engineering and Natural Sciences, Sabancı University, 34956 Istanbul Turkey*

⁴*METU MEMS Center, 06530 Ankara Turkey*

⁵*Faculty of Veterinary Medicine, Department of Virology, Ankara University 06110 Ankara Turkey*

⁶*Biotechnology Institute, Ankara University 06135 Ankara Turkey*

⁷*UNAM — Institute of Materials Science and Nanotechnology, Bilkent University, Turkey*

** These authors contributed equally to this work.*

Abstract

The COVID-19 pandemic highlighted the necessity to develop rapid *in situ* viral detection techniques to isolate infection breakouts. Current biochemical detection techniques, such as polymerase chain reaction (PCR), remain inadequate for initial response due to the delay associated with sequencing the viral genome and reagent development. Alternatively, physical properties of the virus such as mass and size can be quickly profiled and utilized for rapid detection using mass spectrometry (MS). The recent developments in Nanoelectromechanical Systems (NEMS) have made it possible to measure the mass of single particulates with high accuracy; however, significant challenges still exist in adapting NEMS-MS for real biological samples. Sample delivery to the sensing element generally requires the use of delicate vacuum systems and the sensing element suffers from low capture efficiency due to its miniscule size. Here, we develop a NEMS-MS device with an integrated polymeric electrostatic lens to enhance the capture efficiency by several orders-of-magnitude compared to the state-of-the-

art, while allowing for operation under atmospheric conditions. After benchmarking and validating device performance with nanoparticles, we successfully detected the mass of single inactivated SARS-CoV-2 virions from cell lysates with minimum sample preparation. The results establish NEMS technology as an effective approach for the label-free detection of emerging viruses.

Introduction

Standard techniques for detecting viral infections such as polymerase chain reaction (PCR) and immunoassays depend on the knowledge of the specific genetic and biochemical structure of the targeted virus. While the use of genetic and biochemical diagnostic kits has been vital in the response to the current COVID-19 pandemic, the initial development of targeted PCR and antibody-based diagnostic tools inevitably required valuable time for the isolation of the virus, its genetic sequencing, primer development, and the purification and synthesis of SARS-CoV-2 antibodies. Many developed and developing countries faced shortages in testing kits early on during the spread of the pandemic which prevented the efficient isolation of infection pockets and allowed the mixing of asymptomatic carriers with the general population, which in many cases caused the rapid spread of the infection.

A detection technique with a faster response time than current biochemical methods is critically needed to curb future viral outbreaks. One potential technique is to identify a virus based on its mass.¹⁻⁴ The mass of the virus can, in principle, act as a sensing and identification parameter since the length of the genetic sequence and the composition of the capsid are unique for many virus species.

The measurement of the mass of an unknown analyte has traditionally been performed by mass spectrometry⁵⁻⁷ in which analytes are ionised and resolved based on their mass-to-charge (m/z) ratios. If the (m/z) ratio is small, such as in the case of small organic molecules and proteins, accurate measurements can be obtained since the strength of the electromagnetic

interaction compared to the inertia is large, translating to high-resolution mass spectra. On the other hand, if the (m/z) ratio is large, such as the case for large macromolecules and biostructures—including organelles, exosomes, nanoparticles and viruses—top-down characterisation by conventional mass spectrometry becomes much harder, even impossible, since the resolution of the instruments decreases at large (m/z) ratios.

The challenge of weighing large biostructures suffered by conventional mass spectrometry can be met using an emerging mass spectrometry technique based on nanoelectromechanical systems (NEMS). NEMS devices are sensitive to the mass of the species, not their (m/z) ratios. This allows the measurement of species several orders-of-magnitude more massive than what is currently measurable using state-of-the-art conventional MS.⁸ In essence, NEMS devices are vibrating mechanical structures with functional features at the submicron scale (Figure 1).⁹ They are typically made from thin films with excellent mechanical properties, such as silicon nitride on a silicon substrate, and take the form of a suspended beam clamped on one or both of its ends to the substrate. The mechanical vibrations of the beam can be controlled and monitored via electronic signals delivered through addressable gold contacts on either end of the suspended beam.

Owing to their small size, NEMS devices are extremely sensitive to changes in mass. An analyte landing on the active area of NEMS (e.g. the top surface of the suspended beam), increases the mass of the NEMS. Such increases in mass can be accurately determined by monitoring the mechanical resonance frequency of the NEMS which is a function of the total mass of the NEMS. As a result, the landing of analytes on the NEMS translates into a sudden downward shift in the resonance frequency (Figure 1b). Not only do proteins^{10,11} and bacteriophages³ constitute suitable target analytes for NEMS as shown before, mammalian viruses are also prime targets for measurements by NEMS technology since their larger masses (>100 MDa) can give rise to larger frequency shifts, and hence larger signals.

However, several technological barriers still exist for implementing NEMS as virus detectors. Virus detection requires a higher-throughput method for delivering the virion particles to the NEMS device, since the probability of a single virus arriving at the NEMS device is quite low because of its extremely small sensing region (i.e. device surface). In typical NEMS mass spectrometry systems, analyte molecules are generated at atmospheric pressure by soft ionization techniques such as electrospray ionization (ESI), and delivered to the NEMS chip, which is housed inside a complex vacuum system. Not only does the vacuum requirement impede the deployment of NEMS chips in the field, but also intricate setups are necessary to bridge the atmospheric pressure-operated ESI to the vacuum-operated NEMS system to decrease sample loss. The techniques to increase the delivery efficiency of analytes to NEMS involve the use of aerodynamic focusing lenses,³ inertial impaction,¹² the placement of NEMS chips on low-vacuum stages,¹³ and multiplexed detection via an array of devices.¹⁴ However, in all the cases where the literature reported capture efficiency — defined as the ratio of the number of particles detected as a fraction of the total number of particles used in the sample solution divided by the unit area of NEMS device — the values do not exceed one particle out of 8×10^8 particles per μm^2 of sensor area (SI Table S3). This limitation suggests that the use of NEMS technology is impractical for real samples that may contain 10^4 - 10^6 virions per mL. Here, we resolve this major shortcoming in capture efficiency by integrating the NEMS sensor with an on-chip, self-biasing polymeric electrostatic lens that focuses the analyte ions onto the active area of the NEMS device (Figure 1a). Using this arrangement, we have increased the capture efficiency by several orders of magnitude compared to the previous state-of-the-art systems allowing our devices to extract the most out of the active sensing area of any NEMS device.^{3,13} The focused deposition of nanomaterials with the use of polymeric lenses has been studied in the context of parallel nanopatterning¹⁵ and 3D printing¹⁶ whereby nanoparticle structures were fabricated on otherwise blank chips. Here, we transform this

nanoscale deposition technique into a technology for enhancing the delivery of analytes on an active NEMS resonator resulting in a dramatic increase in capture efficiency. To validate the operation of the device, experiments were conducted with 100 nm polystyrene nanoparticles and 20 nm gold nanoparticles to serve as reference analytes due to their known size and concentration. The use of this polymeric electrostatic lens not only increased the capture efficiency, but also allowed us to perform ESI and NEMS-MS sensing entirely under atmospheric conditions where standard ion optics do not work.^{17,18} With the increase in efficiency levels and the elimination of vacuum requirements, a SARS-CoV-2 sample (with a concentration of $\sim 5 \times 10^4$ PFU/mL) was successfully analysed using NEMS mass spectrometry (Figure 1). The versatility of the system was also verified by analysing another mammalian virus, BoHV-1.

Nanoelectromechanical Sensors with Integrated Lenses

The NEMS device is a silicon nitride beam clamped to the silicon substrate from both ends and suspended in air to mechanically vibrate at its resonance frequency. Standard nanofabrication procedures¹⁵ were used to fabricate the beam (15 μ m long, 800 nm wide, 100 nm thick, typically) and deposit gold electrodes on the beam's top surface for integrated electronic transduction.^{19,20} The suspended devices were then spin-coated with a high-viscosity photoresist (AZ 4533) to a final layer thickness of approximately 3.5 μ m. After the deposition of the photoresist, NEMS devices were exposed to ultraviolet (UV) light to open a window in the photoresist layer that was aligned with the active area of the NEMS device (Figure 1d). This way the photoresist surrounds the NEMS structure and forms a polymeric lens to direct the incoming analytes to the active sensing area of the NEMS device. The polymeric focusing lens window in our device architecture is usually 20 microns long by 15 microns wide (SI Section S1).

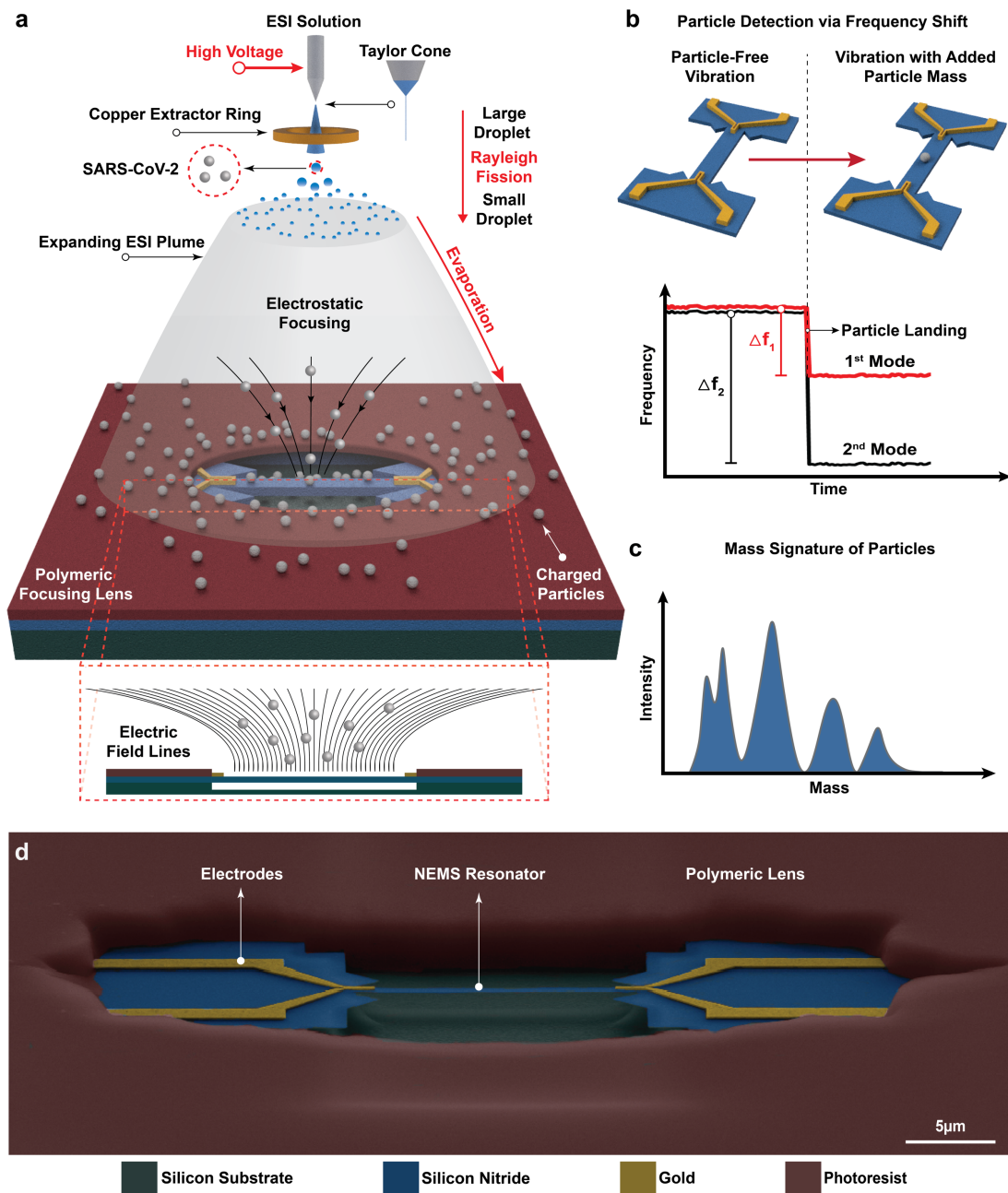


Figure 1: The overall scheme of the sensing system. **(a)** Charged droplets containing the virus are produced by electrospray ionisation. The charged droplets evaporate and undergo Rayleigh fission on their way to the NEMS chip, yielding single virions. The NEMS chip contains the active NEMS device and a photoresist layer having an opening aligned with the active device. The photoresist layer accumulates incoming ions and charges so as to deflect a significant portion of the incoming ions towards the open window, effectively focusing them on the NEMS active area. The illustration is not to scale. **(b)** The incoming virions are then detected by a NEMS device resonating simultaneously in the first two out-of-plane modes so that the mass and position of each incoming virion are detected. **(c)** The measured mass spectrum can be used for species identification. **(d)** A coloured Scanning Electron Microscope (SEM) image of a NEMS device and the surrounding photoresist window. The transduction electrodes are shown in yellow.

In sensing experiments, the NEMS device was vibrated at its mechanical resonance. The mechanical vibration was induced by a time-dependant thermal stress which is actuated by an electrode on one side of the device. By monitoring the piezo-resistive changes in the electrode on the other side of the NEMS device, the mechanical vibration was measured and the resonance frequency of the NEMS device is tracked in real time by a phase-locked loop (PLL) circuit²¹ with a typical Allan deviation of 1×10^{-5} in air. This way, any sudden increase in the device mass induced by the landing of an analyte particle was converted into sudden frequency shifts that can be measured accurately. The frequency shift caused by an analyte depends not only on the mass of the analyte, but also its landing position;²² therefore, we tracked the first two out-of-plane resonance modes of the NEMS device to reverse calculate the landing position of the analyte and to determine its mass.^{11,22-24}

NEMS devices are placed in an in-house prototype setup which involves an electrospray ionisation (ESI) subsystem that generates individual nanoparticles, an extractor lens, and a PCB to hold the NEMS chip itself (Figure 1a, SI Section S4). The entire system is operated at atmospheric pressure in stark contrast with earlier analytical NEMS instruments housed in vacuum. The analyte solution is introduced into the ESI tip by a syringe pump, and a high electrical potential, typically 5.5 kV, is applied to the solution to induce the formation of a Taylor cone at the tip. The extractor lens is held at 1.3 kV. Charged droplets are emitted from the tip and undergo evaporation and Rayleigh fission to yield single analyte ions along their trajectory to the NEMS chip which is located 15 cm away. The NEMS chip is mostly covered by the photoresist, except for the window exposing the NEMS device. Most of the incoming ions initially accumulate on the photoresist surface. However, as more ions accumulate, the steady-state build-up of electrostatic charge causes the ions to deflect towards the open window on the polymeric lens which is aligned with the active area of the NEMS device (SI Section S3).

Nanoparticle Measurements

We first conducted experiments using 100 nm diameter fluorescent polystyrene nanoparticles (Fluoro-Max G100). The fluorescence of the nanoparticles allowed for the visual observation of the position and density of nanoparticles deposited on the NEMS chip using fluorescence microscopy. The concentration of the nanoparticles in this study was 3.55×10^9 per mL in an ammonium acetate buffer (80mM, pH 7.1). Figures 2a clearly indicate successful ionic focusing of particles onto the NEMS sensor; even though some of the particles adhered to the photoresist surface as part of generating and maintaining the electrostatic lensing effect (together with smaller buffer ions produced in ESI).

In addition to fluorescent microscopy, SEM imaging confirms the successful delivery of nanoparticles on the NEMS device (SI Section 2). As each nanoparticle lands on the NEMS device, simultaneous stepwise decreases in both resonance modes are registered (Figure 2b). The mass spectrum of the polystyrene sample was calculated by the frequency shifts and indicates a peak at 384 MDa, which corresponds to a diameter of 103.5 nm (Figure 2b). This value is within the product specifications for the nominally 100 nm polystyrene nanoparticles (size uniformity <10%).

Following that, we decreased the concentration of the particles to 2×10^6 per mL in order to test the focusing performance at the lowest concentration possible while still being able to register events at a reasonable spraying timescale. We observed a capture efficiency of one particle in 371,000 particles per μm^2 , which is equal to one particle in 16,500 particles per device. These results amount to a significant enhancement to the capture efficiency to the current state-of-the-art (SI Section S9). Next, we analysed a sample composed of 20 nm diameter gold nanoparticles (in 80mM ammonium acetate buffer, pH 7.1) with a concentration of 6.54×10^6 particles per mL. In this case, compared with insulating polystyrene nanoparticles, the conductive nanoparticles exhibited far superior focusing ability

(SI Section S9), with a capture efficiency of approximately one nanoparticle in 5600 particles per μm^2 (SI Section S9). Similar differences in the focusing properties of insulating and conductive nanoparticles have been observed within the context of 3D nano-printing.¹⁶

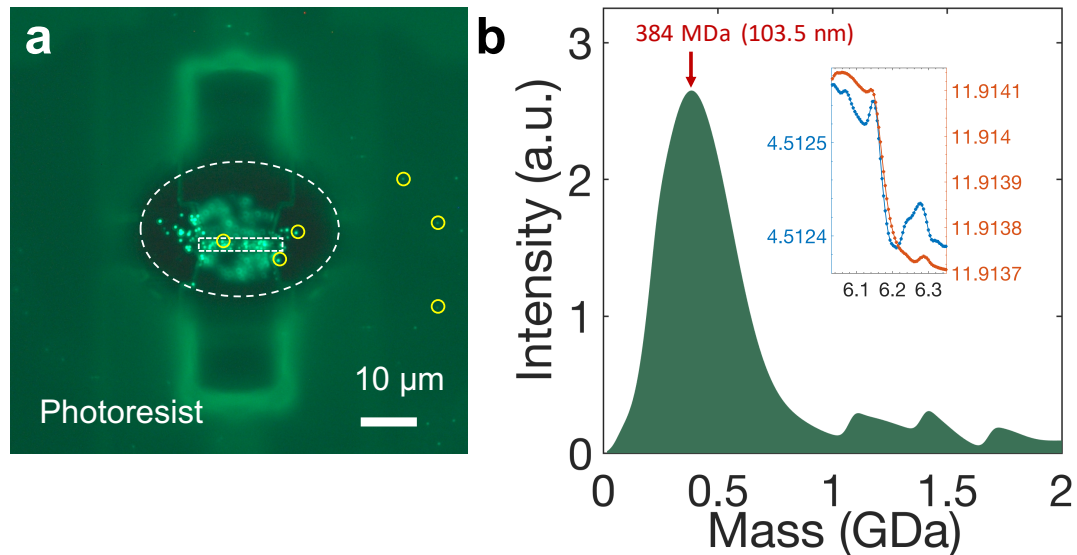


Figure 2: The detection of 100 nm fluorescent polystyrene nanoparticles by NEMS. **(a)** Fluorescence microscopy image showing the efficient focusing of nanoparticles on the NEMS device window. Rectangular dashed area indicates the position of the NEMS beam, oval dashed line shows the window opening on photoresist. For clarity, six particles are highlighted by yellow circles. There are dozens of single particles on the entire image, most of them in the focusing window. Some particles inside the window are out of focal plane in this image since they land at the silicon substrate which is at a lower depth than the NEMS surface. **(b)** The mass spectra obtained by processing the 73 events in the experimental run. The inset shows an example of a single event, with horizontal axis indicating time in seconds, and the left (right) vertical axis indicating the mode 1 (mode 2) frequency in MHz.

SARS-CoV-2 Measurements

Once the system capture efficiency was benchmarked using nanoparticle samples, a SARS-CoV-2 sample, isolated from a COVID-19 patient and expanded *in vitro*, was analysed. The virus sample was harvested by applying a freeze-thaw cycle twice to the cell culture. The cell lysate was then centrifuged to remove cell debris, followed by a short thermal inactivation for safety purposes (Methods, SI Section S5). Before the thermal inactivation, SARS-CoV-2 samples had a concentration of approximately 2×10^6 PFU/mL as calculated by a viral plaque

assay. The virus was isolated using PEG precipitation followed by dialysis at 4°C to exchange the culture media with the ESI-compatible 80 mM ammonium acetate solution (pH 7.1, Methods, SI Section S5). Dynamic Light Scattering (DLS) was then conducted on the sample to obtain the hydrodynamic diameter of the isolated virus in the sample and to confirm the absence of any other major particulates left over from the cell lysate. DLS characterization showed one major peak centred at 86 nm, assumed to correspond to the virion particles, while no other major peaks were detected. The same sample, with virions diluted forty-fold, was then analysed with NEMS MS (Figure 3a), resolving 153 single virion events within 14 minutes. The resulting mass spectrum is shown in Figure 3b which was used to fit a non-parametric probability density function. The global maximum value for the density function is 454 MDa.

To interpret this spectrum, first, we converted the mass values into effective diameter values, assuming that the SARS-COV-2 virions had a spherical shape and using a typical value for the viral mass density (1.4 g/cm³).²⁵ After the conversion, the resulting diameter histogram is shown in Figure 3c, together with the DLS result of the same sample. The peak value for the mass distribution (454 MDa) corresponded to a diameter of 99.7 nm, while the mean diameter was 101.8 nm with a standard deviation of 13.1 nm. The size of SARS-CoV-2 particles has been recently reported²⁶⁻²⁸ by different microscopy techniques (SI Section S10, Table S6) which show that these virion particles have a mean diameter in the range of 90-94 nm with standard deviations close to 10 nm (8 nm -13.7 nm). Most of the aforementioned studies report the size values without the peplomers, while NEMS measurements include the entire structure: hence, it is expected that the size reported by NEMS MS is larger. The similarity of the values indicates that the NEMS MS system, operating at room temperature and atmospheric pressure, can rapidly determine the mass signature of the virions which would

allow to isolate any infected person from the crowds in the early stage of a possible future pandemic.

After this additional verification, PEG precipitation was removed from the protocol to check the performance of the NEMS on a relatively complex biological solution such as the clarified cell lysate. The cell lysate was subjected to dialysis in order to remove any non-volatile salts for ESI. The DLS analysis of the lysate showed a peak near 115 nm coalescing with a much larger peak spanning 200-1200 nm presumably owing to the interference of cellular debris in the sample. Spraying such a solution containing relatively massive particulates can potentially damage the suspended NEMS beam. This was what we observed in several runs, where the device stopped responding after a few minutes of ESI presumably due to damage. This can be remedied by centrifuging the cell lysate for longer or at a higher speed than in the described protocol to remove the majority of the larger cell debris. On such a trial, a total of 101 events were registered after approximately 18 minutes of spraying. Most of these events fell on the mass range determined from the isolated SARS-CoV-2 sample (Figure 3d). Compared to the isolated virus sample, there were additional materials especially at the higher mass values, presumably originating from the cellular debris. However, above this background, a clear, population emerged at the expected location for SARS-CoV-2 with the major peak almost overlapping with the peak of the spectrum of the isolated virus (469 vs. 454 MDa respectively, for further statistics, SI Table S5).

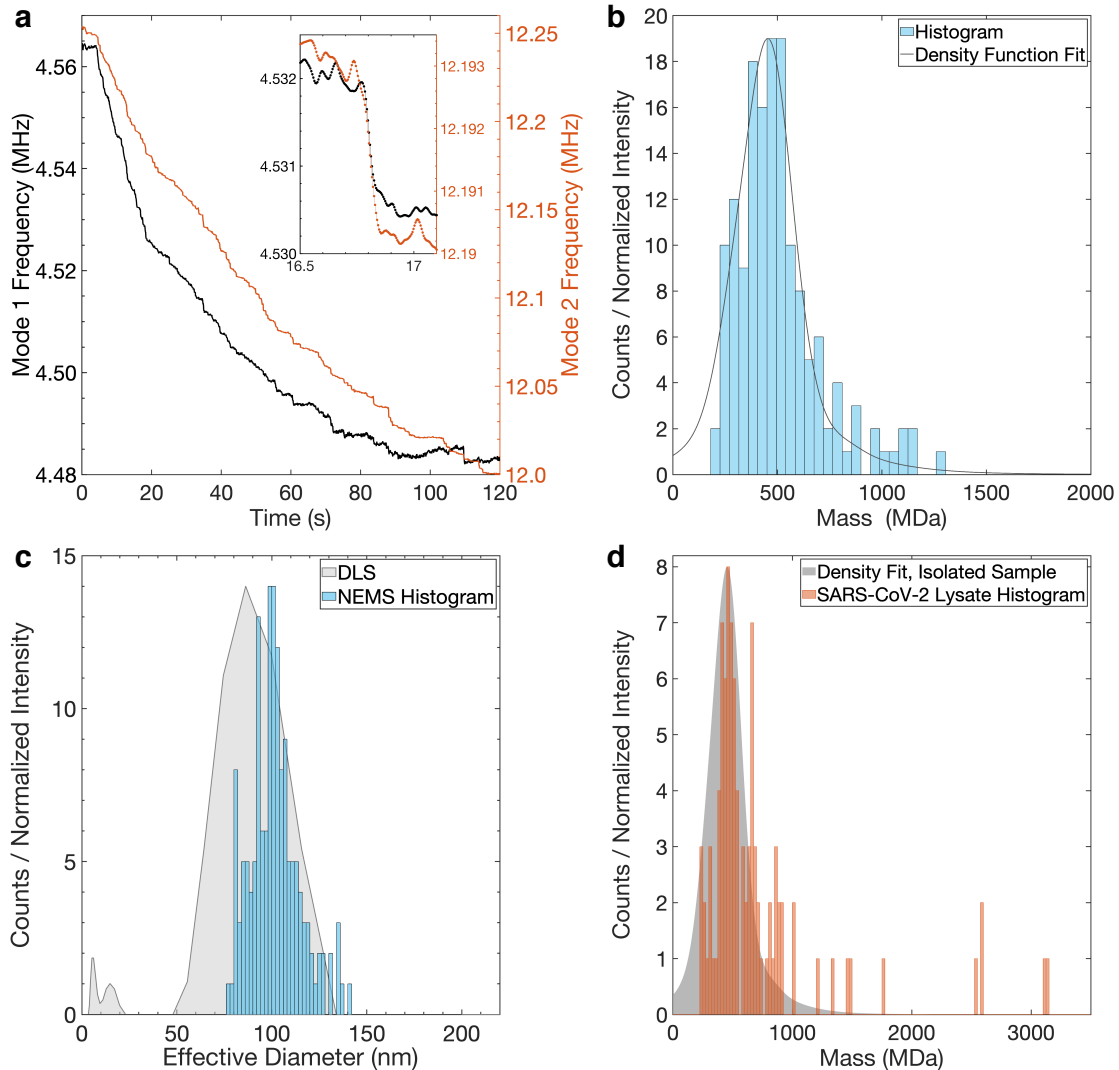


Figure 3: Single SARS-CoV-2 virion mass sensing. **(a)** Raw data for the frequency tracking in two modes. Simultaneous shifts in two modes corresponding to SARS-CoV-2 virions landing on the NEMS device. The inset shows one event close-up. **(b)** The mass spectrum accumulated after 153 landing events for SARS-CoV-2. A non-parametric density function is fitted to the histogram. **(c)** Corresponding diameter histogram calculated by the assumption that the virus density is 1.4 g/cm^3 shown together with the DLS analysis result for the same sample. **(d)** Orange: the mass spectra histogram of a SARS-CoV-2 lysate obtained without isolating the virus using PEG precipitation. Grey: the mass spectra density function of the isolated sample in (b) rescaled along the y-axis to show the degree of overlap between the two experiments.

Furthermore, we analysed an inactivated BoHV-1 sample, processed in the same manner as the isolated SARS-CoV-2 sample, to both act as a control experiment and show our system's capability of detecting virions from a different mammalian virus family. This virus has a more complex structure compared to SARS-CoV-2 and has a larger mean diameter and a broad size

distribution studied by electron microscopy.²⁹ The NEMS MS results in this case agreed with the expected size distribution of BoHV-1 (SI Section S8). More importantly, specific peaks near the expected mass and size values that emerged from the SARS-CoV-2 analyses were not present in the run conducted with BoHV-1.

It was not possible to measure the actual virion concentration prior to ESI, since the standard technique of plaque assay quantifies only the active viruses. Therefore, assessing the capture efficiency achieved through NEMS detection for the particular case of SARS-CoV-2 was not possible. Nevertheless, this work clearly establishes that NEMS Mass Spectrometry can now be used in more realistic and relevant biological samples with concentrations as low as 5×10^4 PFU/mL, and sample volumes as little as 7 μ L. Moreover, this analysis can also be done directly on complex media such as a cell lysate which eliminates the necessity for complex sample preparations. Ambient NEMS MS can potentially form the core of a rapid screening tool for novel viral threats that is not reliant on genomic sequencing. Such a system will be of critical importance to the rapid tracking and isolation of individuals whose test samples exhibit mass fingerprints that correspond to the identified novel viral strain.

Conclusion

With the technique and results presented here, one of the main challenges in using NEMS sensors for real-world applications has been resolved, namely, the increase in analyte capture efficiency per active sensing area by many orders of magnitude under atmospheric pressure. With the increase in capture efficiency per area, the use of a physical sensor for the direct detection of virus-infections at point-of-care has become feasible. As such, commercially viable products, which are not bogged down by the complexities and cost of vacuum operated devices, can now be manufactured.

To further improve the specificity of virus detection, another important challenge for NEMS technology, a biochemical protocol may be carried out to dissolve away the external lipid shell of the virus. The nucleocapsid along with the associated RNA provides a mass fingerprint that is more unique to virus species than the mass of the whole virion which can vary based on the host cell. We also believe that this technique has applicability beyond the context presented here. For instance, the integration of self-focusing NEMS chips within air conditioning systems can enable the surveillance of nanoparticle density to establish the existence of potential viral threats and particulate pollution, especially if the mass density information is obtained using an even larger number of mechanical vibration modes.²⁴ Additionally, RNA viruses like HIV, influenza, and SARS-CoV-2 tend to pick up mutations quickly due to the error-prone RNA-copying enzymes. These mutations typically affect viral surface protein sequences, potentially rendering immunoassay detection kits ineffective for mutated strains. Nonetheless, total mass remains highly conserved, allowing mass-based detection to be a more robust approach. NEMS mass spectrometry can become an ideal detection method for this purpose.

Methods

Electrospray Ionization: ESI tips (New Objective) were used with tip diameters as either 10 μm or 30 μm . An extractor lens (50 \times 50 mm square copper plate with a 15 mm diameter hole) was used at a distance (typically 4-6 mm) away from the tip. The typical ESI voltages for the tip was 5.5 kV and 1.3 kV for the extractor using separate high voltage sources for each component (High voltage fluidic connector: American Power Design, Inc. P2-600/C/Y, controlled by Agilent E3640A; Extractor: Emco High Voltage -E60, controlled by Marxlow RXN-1502D). The NEMS chip has been placed typically at 75-150 mm away from the tip.

ESI flow rate of 500 nL/min was used and the flow was supplied by a syringe pump (New Era Pump Systems, Inc. NE-1000).

Cell lysate preparation for ESI

Frozen samples of SARS-CoV-2 infected Vero E6 cell lysate was provided by Ankara University. The lysate was thawed and treated with a PEG virus precipitation kit to isolate the virus from the remainder of the cell debris. Following precipitation, the virus isolates were dialyzed against ammonium acetate buffer to remove non-volatile salts left over from the cell culture media. Details of the cell lysate preparation are available in the SI methods section. Finally, methanol was added to the isolated virus solution to a concentration of 10% (v/v) to facilitate the ESI process.

BoHV-1 cell lysate samples were also received from Ankara University and treated following the same procedure outlined above.

SARS-CoV-2 cell lysate that was not PEG concentrated was directly dialyzed against ammonium acetate as detailed in the SI methods section, supplemented with methanol (10% v/v), and used directly for ESI.

Data Availability Statement

The data that support the findings of this study are available from the corresponding author upon reasonable request.

Code Availability Statement

The code that support the findings of this study are available from the corresponding author upon reasonable request.

References

- 1 Wick, C. H. *Integrated Virus Detection*. (CRC Press, 2014).
- 2 Burg, T. P. *et al.* Weighing of biomolecules, single cells and single nanoparticles in fluid. *Nature* **446**, 1066-1069 (2007).
- 3 Dominguez-Medina, S. *et al.* Neutral mass spectrometry of virus capsids above 100 megadaltons with nanomechanical resonators. *Science* **362**, 918-922 (2018).
- 4 Ruz, J., Tamayo, J., Pini, V., Kosaka, P. & Calleja, M. Physics of nanomechanical spectrometry of viruses. *Scientific Reports* **4**, 1-11 (2014).
- 5 Fenn, J. B., Mann, M., Meng, C. K., Wong, S. F. & Whitehouse, C. M. Electrospray ionization for mass spectrometry of large biomolecules. *Science* **246**, 64-71 (1989).
- 6 Tanaka, K. *et al.* Protein and polymer analyses up to m/z 100 000 by laser ionization time-of-flight mass spectrometry. *Rapid Communications in Mass Spectrometry* **2**, 151-153 (1988).
- 7 Karas, M., Bachmann, D. & Hillenkamp, F. Influence of the wavelength in high-irradiance ultraviolet laser desorption mass spectrometry of organic molecules. *Analytical Chemistry* **57**, 2935-2939 (1985).
- 8 Wörner, T. P. *et al.* Resolving heterogeneous macromolecular assemblies by Orbitrap-based single-particle charge detection mass spectrometry. *Nature Methods* **17**, 395-398 (2020).
- 9 Craighead, H. G. Nanoelectromechanical systems. *Science* **290**, 1532-1535 (2000).
- 10 Naik, A. K., Hanay, M. S., Hiebert, W. K., Feng, X. L. & Roukes, M. L. Towards single-molecule nanomechanical mass spectrometry. *Nature Nanotechnology* **4**, 445-450, doi:10.1038/nnano.2009.152 (2009).
- 11 Hanay, M. S. *et al.* Single-protein nanomechanical mass spectrometry in real time. *Nature Nanotechnology* **7**, 602-608, doi:10.1038/nnano.2012.119 (2012).

- 12 Schmid, S., Kurek, M., Adolphsen, J. Q. & Boisen, A. Real-time single airborne nanoparticle detection with nanomechanical resonant filter-fiber. *Scientific Reports* **3**, 1288 (2013).
- 13 Malvar, O. *et al.* Mass and stiffness spectrometry of nanoparticles and whole intact bacteria by multimode nanomechanical resonators. *Nature Communications* **7**, 1-8 (2016).
- 14 Sage, E. *et al.* Single-particle mass spectrometry with arrays of frequency-addressed nanomechanical resonators. *Nature Communications* **9**, 1-8 (2018).
- 15 Kim, H. *et al.* Parallel patterning of nanoparticles via electrodynamic focusing of charged aerosols. *Nature Nanotechnology* **1**, 117-121 (2006).
- 16 Zhu, Y. & Chiarot, P. R. Directed assembly of nanomaterials using electrospray deposition and substrate-level patterning. *Powder Technology* (2020).
- 17 Baird, Z., Wei, P. & Cooks, R. G. Ion creation, ion focusing, ion/molecule reactions, ion separation, and ion detection in the open air in a small plastic device. *Analyst* **140**, 696-700 (2015).
- 18 Baird, Z., Peng, W.-P. & Cooks, R. G. Ion transport and focal properties of an ellipsoidal electrode operated at atmospheric pressure. *International Journal of Mass Spectrometry* **330**, 277-284 (2012).
- 19 Li, M., Tang, H. X. & Roukes, M. L. Ultra-sensitive NEMS-based cantilevers for sensing, scanned probe and very high-frequency applications. *Nature Nanotechnology* **2**, 114-120, doi:10.1038/nnano.2006.208 (2007).
- 20 Bargatin, I., Kozinsky, I. & Roukes, M. L. Efficient electrothermal actuation of multiple modes of high-frequency nanoelectromechanical resonators. *Applied Physics Letters* **90**, 093116, doi:10.1063/1.2709620 (2007).

- 21 Demir, A. & Hanay, M. S. Fundamental Sensitivity Limitations of Nanomechanical Resonant Sensors Due to Thermomechanical Noise. *IEEE Sensors Journal* **20**, 1947-1961 (2019).
- 22 Dohn, S., Svendsen, W., Boisen, A. & Hansen, O. Mass and position determination of attached particles on cantilever based mass sensors. *Review of Scientific Instruments* **78**, 103303 (2007).
- 23 Hanay, M. S. *et al.* Inertial imaging with nanomechanical systems. *Nature Nanotechnology* **10**, 339-344 (2015).
- 24 Sader, J. E., Hanay, M. S., Neumann, A. P. & Roukes, M. L. Mass spectrometry using nanomechanical systems: beyond the point-mass approximation. *Nano Letters* **18**, 1608-1614 (2018).
- 25 Francis, Z. *et al.* Monte Carlo simulation of SARS-CoV-2 radiation-induced inactivation for vaccine development. *arXiv preprint arXiv:2005.06201* (2020).
- 26 Laue, M., Kauter, A., Hoffmann, T., Michel, J. & Nitsche, A. Morphometry of SARS-CoV and SARS-CoV-2 particles in ultrathin sections of infected Vero cell cultures. *bioRxiv* (2020).
- 27 Klein, S. *et al.* SARS-CoV-2 structure and replication characterized by in situ cryo-electron tomography. *Nature Communications* **11**, 1-10 (2020).
- 28 Ke, Z. *et al.* Structures and distributions of SARS-CoV-2 spike proteins on intact virions. *Nature* **588**, 498-502, doi:10.1038/s41586-020-2665-2 (2020).
- 29 Ludwig, H. in *The Herpesviruses: Volume 2* (ed Bernard Roizman) 135-214 (Springer US, 1983).

Acknowledgements: This work was supported by the Scientific and Technological Research Council of Turkey (*TÜBİTAK*), Grant No. EEEAG-119E503. M. S. H. acknowledges indirect support from ERC Starting Grant REM 758769, and fellowship supports from TÜBA and The Science Academy, Turkey. The authors thank Sabancı University SUNUM for nanofabrication support. The Authors thank Urartu Seker, Berk Kucukoglu, Uzay Tefek, Peyman Firoozy, Kadir Ulak, Yagmur Ceren Alatas, Ece Kayacilar and Sakir Duman for useful discussions.

Author Contributions The manuscript was written through contributions of all authors. All authors have given approval to the final version of the manuscript. M.S.H. conceived the idea; R.T.E, B.E.K., M.K., M.A, I.K. developed new ideas for the instrumentation; H.A., B.E.K., M.A. processed the nanoparticle and virus samples; R.T.E., M.A. and B.E.K. operated the NEMS MS system and took the data; H.S.P. and C.Y. performed nano-fabrication; M.K., A.M.Y., B.E.K, I.K., R.T.E. and B.S. performed packaging; B.E.K., R.T.E., and H.S. P. designed the NEMS devices; Z.B.S., M.A., I.K. and M.K. performed the data analysis; H. A. developed the necessary protocols for virus isolation, and performed confirmatory analysis (DLS, UV/Vis). H. A. contributed to writing and preparation of the manuscript A.O. provided the virus samples and provided consultation on viral preparations.

Competing Interests: MSH and RTE are cofounders of *Sensonance*; the other authors declare no competing interests.

Additional information

Correspondence and requests for materials should be addressed to M.S.H.